EUROPEAN ORGANIZATION FOR NUCLEAR RESEARCH

CERN-EP/2001-065
September 7, 2001

Inclusive π^0 and K^0_S Production in Two-Photon Collisions at LEP

The L3 Collaboration

Abstract

The reactions $e^+e^- \to e^+e^-\pi^0$ X and $e^+e^- \to e^+e^-K^0_S$ X are studied using data collected at LEP with the L3 detector at centre-of-mass energies between 189 and 202 GeV. Inclusive differential cross sections are measured as a function of the particle transverse momentum p_t and the pseudo-rapidity. For $p_t \leq 1.5$ GeV, the π^0 and K^0_S differential cross sections are described by an exponential, typical of soft hadronic processes. For $p_t \geq 1.5$ GeV, the cross sections show the presence of perturbative QCD processes, described by a power-law. The data are compared to Monte Carlo predictions and to NLO QCD calculations.

Submitted to *Phys. Lett. B*

1 Introduction

Two-photon collisions are the main source of hadron production in the high-energy regime of LEP via the process $e^+e^- \to e^+e^- \gamma^*\gamma^* \to e^+e^- hadrons$. In the Vector Dominance Model, each photon can transform into a vector meson with the same quantum numbers, thus initiating a strong interaction process with characteristics similar to hadron-hadron interactions. This process dominates in the "soft" interaction region, where hadrons are produced with a low transverse momentum p_t. Hadrons with high p_t are produced by the direct QED process $\gamma^*\gamma^* \to q\bar{q}$ or by QCD processes originating from the partonic content of the photon. QCD calculations are available for single particle inclusive production in two-photon interactions at next-to-leading order (NLO) [1, 2].

In this letter, inclusive π^0 and K^0_S production from quasi-real photons is studied for a centre-of-mass energy of the two interacting photons, $W_{\gamma\gamma}$, greater than 5 GeV. The π^0's are measured in the transverse momentum range $0.2 \leq p_t \leq 20$ GeV and in the pseudo-rapidity[1)] interval $|\eta| \leq 4.3$. The K^0_S's are measured in the range $0.4 \leq p_t \leq 4$ GeV and $|\eta| \leq 1.5$.

The data used for this analysis were collected by the L3 detector [3] at centre-of-mass energies from $\sqrt{s} = 189$ GeV to 202 GeV, with a luminosity weighted average value of $\sqrt{s} = 194$ GeV. The integrated luminosity is 414 pb^{-1}. Previous measurements of inclusive charged hadron and K^0_S production were performed at LEP [4] at $\sqrt{s} = 161 - 172$ GeV.

2 Monte Carlo simulation

The process $e^+e^- \to e^+e^- hadrons$ is modelled with the PHOJET [5] and PYTHIA [6] event generators with respectively 2 and 3 times more luminosity than the data. The following generators are used to simulate background processes: PYTHIA and KK2f [7] for $e^+e^- \to q\bar{q}\,(\gamma)$; KORALZ [8] for $e^+e^- \to \tau^+\tau^-(\gamma)$; KORALW [9] for $e^+e^- \to W^+W^-$ and DIAG36 [10] for $e^+e^- \to e^+e^-\tau^+\tau^-$. The events are simulated in the L3 detector using the GEANT [11] and GEISHA [12] programs and passed through the same reconstruction program as the data. Time dependent detector inefficiencies, as monitored during the data taking period, are also simulated.

3 Event selection

The selection of $e^+e^- \to e^+e^- hadrons$ events is based on information from the central tracking detectors and from the electromagnetic (BGO) and hadronic calorimeters [13]. In order to restrict the Q^2 interval, we exclude events with a cluster in the small-angle calorimeter with energy greater than 30 GeV. About 2 million hadronic events are selected. The level of background is less than 1% and is mainly due to the $e^+e^- \to q\bar{q}\,(\gamma)$ and $e^+e^- \to e^+e^-\tau^+\tau^-$ processes.

The particle identification proceeds from charged tracks and electromagnetic clusters. The inner tracking detector extends up to $|\eta| = 1.64$. The electromagnetic calorimeters extend up to $|\eta| \leq 0.96$ for the barrel, and cover $1.15 \leq |\eta| \leq 2.25$ for the endcaps and $3.37 \leq |\eta| \leq 4.38$ for the small-angle detector. A track must have a transverse momentum above 100 MeV and a distance of closest approach to the primary vertex in the transverse plane below 10 mm. An electromagnetic cluster must have an energy greater than 100 MeV formed by the energy deposited in at least 2 neighbouring BGO crystals. There should be no charged track within an

[1)] $\eta = -\ln\ \tan(\theta/2)$, where θ is the polar angle of the particle relative to the beam axis.

angle of 200 mrad and the associated energy in the hadron calorimeter must be less than 20% of the electromagnetic energy. Clusters in the small-angle detector must have an energy greater than 2 GeV and restrictions on the energy profile in each cluster are applied to distinguish well reconstructed photons from those at the edges of the detector or from residual hadrons.

For $p_t < 5$ GeV, the inclusive π^0 production is measured via the decay of the π^0 into two photons associated to two electromagnetic clusters. The distribution of the effective mass of the reconstructed $\gamma\gamma$ system shows a clear π^0 peak in all the detector regions. Examples for the central region and the small-angle detector are given in Figures 1a and 1b, respectively. Over the entire range of $|\eta|$ and p_t, the resolution varies between 6.6 and 13.5 MeV, and is well reproduced by Monte Carlo simulation. For $p_t > 4$ GeV and $|\eta| < 0.5$, the two final photons are unresolved and the π^0 is associated to a single electromagnetic cluster. To avoid double-counting in the region $4 < p_t < 5$ GeV and $|\eta| < 0.5$, where both methods are applied, only clusters which do not contribute to combinations in a 3-σ mass band around the π^0 peak are taken into account. In this region, we have checked that the two methods applied separately agree within errors.

Inclusive $\mathrm{K^0_S}$ production is measured using the decay $\mathrm{K^0_S} \to \pi^+\pi^-$ that produces two oppositely charged tracks. The $\mathrm{K^0_S}$'s are selected by reconstructing the secondary decay vertex. The projected distance, in the transverse plane, between the secondary vertex and the primary $\mathrm{e^+e^-}$ interaction point is required to be greater than 3 mm. The angle between the projected flight direction of the $\mathrm{K^0_S}$ candidate and the total transverse momentum vector of the two outgoing tracks must be less than 75 mrad. After these cuts, about 5×10^5 events are selected. The distribution of the effective mass of the reconstructed $\pi^+\pi^-$ system shows a clear $\mathrm{K^0_S}$ peak. Examples for different p_t bins are given in Figures 1c and 1d. The resolution varies from 8 MeV for $p_t < 1$ GeV to 10 MeV around 4 GeV, and is well reproduced by Monte Carlo simulation.

4 Differential cross sections

Differential cross sections as a function of the transverse momentum p_t and of the absolute pseudorapidity $|\eta|$ are calculated using the number of π^0 and $\mathrm{K^0_S}$ candidates and the overall efficiency for each bin of p_t or $|\eta|$. The overall efficiency includes reconstruction and trigger efficiencies and takes into account the branching fraction of the $\mathrm{K^0_S}$ into $\pi^+\pi^-$. The reconstruction efficiency includes the effects of the acceptance and selection cuts and is calculated with the Monte Carlo generators PHOJET and PYTHIA. As both generators reproduce well the shapes of the experimental distributions of hadronic two-photon production [13], their average is used.

Two-photon events are collected predominantly by the track triggers [14]. The trigger efficiency is derived from each year's data sample by comparing the number of events accepted by the independent track and calorimetric energy [15] triggers. The efficiencies of higher level triggers are measured using prescaled events. For the π^0, it varies from 80% at low p_t to 100% at high p_t. For the $\mathrm{K^0_S}$, it is 85% independently of p_t.

The cross sections are calculated for $\mathrm{W_{\gamma\gamma}} \geq 5$ GeV and a photon virtuality $Q^2 \leq 8$ GeV^2. The overall efficiency does not depend on the Q^2 cutoff.

4.1 $\mathrm{e^+e^- \to e^+e^-\pi^0}$ X analysis

To evaluate the number of π^0's when the two photons are well separated in the detector, fits are made to the $\gamma\gamma$ mass distribution in the interval $50 < M_{\gamma\gamma} < 200$ MeV using a Gaussian

to describe the signal and a third degree Chebyshev polynomial for the background. All the parameters, including mass and width of the peak, are left free.

When single clusters are identified as a π^0, the contamination coming from the decays of other mesons (η, ω, η',...) is on average 15.1 ± 1.2 % over the entire p_t and $|\eta|$ ranges. Single photon production ($\gamma q \to \gamma q$, $q\bar{q} \to \gamma g$, $gq \to \gamma q$) is predicted to be more than one order of magnitude below our measurements [16]. In addition, a study of the energy profile of each cluster reveals no significant background from this source. The background due to annihilation events increases with p_t up to a maximum of 11 %.

The reconstruction efficiency varies between 15% and 50% in the different p_t and $|\eta|$ ranges. The efficiency increases from $p_t \simeq 0.2$ GeV, where a low energy photon can go undetected, up to $p_t \simeq 2$ GeV. In the region $2 < p_t < 4$ GeV, the efficiency decreases due to the increasing percentage of events in which the two photons merge. For $p_t > 4$ GeV, the addition of the single-cluster analysis gives a higher efficiency. The efficiency decreases with polar angle due to the acceptance of the calorimeters.

Sources of systematic uncertainties on the cross-section measurements are selection criteria, Monte Carlo modelling, background subtraction and accuracy of the trigger efficiency measurement. The uncertainty due to selection criteria is dominated by hadron selection, estimated to be 7.5 % [13]. The Monte Carlo modelling uncertainty, taken as half the relative difference between PHOJET and PYTHIA, increases with p_t from 1% to 24%. The background uncertainty varies from 5% to 15% for $p_t < 5$ GeV. It is estimated using different background parametrisations during the fitting procedure. In the high p_t region, the uncertainty on the annihilation background subtraction is taken as half the difference between PYTHIA and KK2f and varies from 0.1% to 5%. The uncertainty on the trigger efficiency varies from 0.1% to 1.1% due to the statistical accuracy of its determination.

The overall efficiencies and differential cross sections $d\sigma/dp_t$ and $d\sigma/d|\eta|$ are given in Tables 1 and 2. The π^0 multiplicity in the range $0.2 < p_t < 20$ GeV and $|\eta| < 0.5$ is $0.275 \pm 0.001 \pm 0.025$ per $e^+e^- \to e^+e^-$*hadrons* event, in agreement with Monte Carlo predictions, 0.281 for PHOJET and 0.285 for PYTHIA.

4.2 $e^+e^- \to e^+e^-K^0_S$ X analysis

The number of K^0_S is evaluated by means of a fit to the $\pi^+\pi^-$ mass distribution in the interval $400 < M_{\pi^+\pi^-} < 600$ MeV. A Gaussian describes the signal and a third degree Chebyshev polynomial the background. All parameters, including the mass and width of the peak, are left free.

The reconstruction efficiency is of the order of 20 %. Systematic uncertainties, estimated as in the π^0 case, are selection criteria (7.5%), Monte Carlo modelling (1−6%), background subtraction (1−7%) and trigger efficiency measurement accuracy (2%). In addition, a 2.5 % uncertainty arises from the K^0_S selection criteria.

The overall efficiencies and differential cross sections $d\sigma/dp_t$ and $d\sigma/d|\eta|$ are given in Tables 3 and 4. The multiplicity of K^0_S in the range $0.4 < p_t < 4$ GeV and $|\eta| < 1.5$ is $0.060 \pm 0.006 \pm 0.003$ per $e^+e^- \to e^+e^-$*hadrons* event, in agreement with Monte Carlo predictions, 0.067 for PHOJET and 0.056 for PYTHIA.

5 Results

Differential cross sections of π^0 and K^0_S production with respect to p_t and $|\eta|$ are shown in Figures 2, 3 and 4.

The behaviour of $d\sigma/dp_t$ in the range $0.2 < p_t < 1.5$ GeV for π^0 and $0.6 < p_t < 1.5$ GeV for K^0_S is described by an exponential of the form $Ae^{-p_t/\langle p_t\rangle}$ with a mean value of $\langle p_t\rangle \simeq 230$ MeV for the π^0 and $\langle p_t\rangle \simeq 290$ MeV for the K^0_S. This behaviour is characteristic of hadrons produced by soft interactions and is similar to that obtained in hadron-hadron and photon-hadron collisions [17]. Due to the direct $\gamma\gamma \to q\bar{q}$ process and to hard QCD interactions, two-photon collisions exhibit a cross section higher than the expected exponential behaviour at high p_t values. For $p_t \geq 1.5$ GeV, the differential cross sections are better represented by a power law function Ap_t^{-B}. The value of the power B is compatible with 4 for both π^0 and K^0_S. In the framework of Reference [18], this value is expected in the case of $2 \to 2$ hard scattering processes at the parton level.

The differential cross sections are also compared to Monte Carlo predictions in Figure 2. In the π^0 case, the high p_t region is not reproduced by PYTHIA nor by PHOJET. We verify that the shapes of the $|\eta|$ distributions of π^0 and K^0_S are well reproduced by both models.

In Figures 3a and 3b the data are compared to analytical NLO QCD predictions [19]. For this calculation, the flux of quasi-real photons is obtained using the Equivalent Photon Approximation, taking into account both transverse and longitudinal virtual photons. The interacting particles can be photons or partons from the $\gamma \to q\bar{q}$, which evolves into quarks and gluons. The NLO parton density functions of Reference [20] are used and all elementary $2 \to 2$ and $2 \to 3$ processes are considered. New NLO fragmentation functions (FF) [21] are used assuming that $FF(\pi^0) = (FF(\pi^+) + FF(\pi^-))/2$. The renormalization, factorisation and fragmentation scales are taken to be equal: $\mu = M = M_F = \xi p_t$ [2]. The scale uncertainty in the NLO calculation is estimated by varying the value of ξ from 0.5 to 2.0. The structure in the p_t spectrum for the K^0_S calculation is due to the charm threshold in the fragmentation function [2, 22]. The agreement with the data is satisfactory in the K^0_S case, but it is poor for the π^0 case in the high-p_t range.

The $d\sigma/d|\eta|$ differential cross sections, are also compared to QCD calculations as shown in Figure 4. The shape of the data, and in particular the measurement of the π^0 production at $\langle|\eta|\rangle = 3.85$, is reproduced by NLO QCD predictions.

Acknowledgements

We would like to thank B. A. Kniehl, L. Gordon and M. Fontannaz for providing us with their NLO QCD calculations and R. Engel and T. Sjöstrand for useful discussions.

References

[1] L. E. Gordon, Phys. Rev. **D 50** (1994) 6753.

[2] J. Binnewies, B. A. Kniehl and G. Kramer, Phys. Rev. **D 53** (1996) 6110.

[3] L3 Coll., B. Adeva et al., Nucl. Instr. Meth. **A 289** (1990) 35; L3 Coll., M. Acciarri et al., Nucl. Instr. Meth. **A 351** (1994) 300.

[4] OPAL Coll., G. Abbiendi *et al.*, Eur. Phys. J. **C 6** (1999) 253.

[5] PHOJET version 1.05c is used;
R. Engel, Z. Phys. **C 66** (1995) 203 ;
R. Engel and J. Ranft, Phys. Rev. **D 54** (1996) 4246;
R. Engel private communication.

[6] PYTHIA version 5.722 and JETSET version 7.409 are used;
T. Sjöstrand, Comp. Phys. Comm. **82** (1994) 74.

[7] KK2f version 4.12 is used;
S. Jadach, B. F. L. Ward Z. Wąs, Comp. Phys. Comm. **130** (2000) 260.

[8] S. Jadach, B. F. L. Ward and Z. Wąs, Comp. Phys. Comm. **79** (1994) 503.

[9] M. Skrzypek, S. Jadach, W. Placzek, and Z. Wąs, Comp. Phys. Comm. **94** (1996) 216.

[10] F. A. Berends, P. H. Daverfeldt and R. Kleiss, Nucl. Phys. **B 253** (1985) 441.

[11] R. Brun et al., GEANT 3.15 preprint CERN DD/EE/84-1 (1984), revised 1987.

[12] H. Fesefeldt, RWTH Aachen report PITHA 85/2 (1985).

[13] L3 Coll., M. Acciarri *et al.*, preprint hep-ex/0102025 (2001), to be published in Phys. Lett.

[14] P. Béné et al., Nucl. Instr. Meth. **A 306** (1991) 150;
D. Haas et al., Nucl. Instr. Meth. **A 420** (1999) 101.

[15] R. Bizzarri *et al.*, Nucl. Instr. Meth. **A 283** (1989) 799.

[16] L. E. Gordon and J. K. Storrow, Phys. Lett. **B 385** (1996) 385;
M. Fontannaz, private communication.

[17] M. L. Perl, *High Energy Hadron Physics* (ed. John Wiley, New-York, 1974).

[18] S. J. Brodsky and G. R. Farrar, Phys. Rev. Lett. **31** (1973) 1153.

[19] B. A. Kniehl, private communication.

[20] P. Aurenche, J.-P. Guillet, M. Fontannaz, Zeit. Phys. **C 64** (1994) 621.

[21] B. A. Kniehl, G. Kramer and B. Pötter, Nucl. Phys. **B 582** (2000) 514.

[22] J. Binnewies, B. A. Kniehl and G. Kramer, Phys. Rev. **D 52** (1995) 4947.

Author List

The L3 Collaboration:

P.Achard,[20] O.Adriani,[17] M.Aguilar-Benitez,[24] J.Alcaraz,[24,18] G.Alemanni,[22] J.Allaby,[18] A.Aloisio,[28] M.G.Alviggi,[28] H.Anderhub,[47] V.P.Andreev,[6,33] F.Anselmo,[9] A.Arefiev,[27] T.Azemoon,[3] T.Aziz,[10,18] M.Baarmand,[25] P.Bagnaia,[38] A.Bajo,[24] G.Baksay,[16]L.Baksay,[25] S.V.Baldew,[2] S.Banerjee,[10] Sw.Banerjee,[4] A.Barczyk,[47,45] R.Barillère,[18] P.Bartalini,[22] M.Basile,[9] N.Batalova,[44] R.Battiston,[32] A.Bay,[22] F.Becattini,[17] U.Becker,[14] F.Behner,[47] L.Bellucci,[17] R.Berbeco,[3] J.Berdugo,[24] P.Berges,[14] B.Bertucci,[32] B.L.Betev,[47] M.Biasini,[32] M.Biglietti,[28] A.Biland,[47] J.J.Blaising,[4] S.C.Blyth,[34] G.J.Bobbink,[2] A.Böhm,[1] L.Boldizsar,[13] B.Borgia,[38] S.Bottai,[17] D.Bourilkov,[47] M.Bourquin,[20] S.Braccini,[20] J.G.Branson,[40] F.Brochu,[4] A.Buijs,[43] J.D.Burger,[14] W.J.Burger,[32] X.D.Cai,[14] M.Capell,[14] G.Cara Romeo,[9] G.Carlino,[28] A.Cartacci,[17] J.Casaus,[24] F.Cavallari,[38] N.Cavallo,[35] C.Cecchi,[32] M.Cerrada,[24] M.Chamizo,[20] Y.H.Chang,[49] M.Chemarin,[23] A.Chen,[49] G.Chen,[7] G.M.Chen,[7] H.F.Chen,[21] H.S.Chen,[7] G.Chiefari,[28] L.Cifarelli,[39] F.Cindolo,[9] I.Clare,[14] R.Clare,[37] G.Coignet,[4] N.Colino,[24] S.Costantini,[38] B.de la Cruz,[24] S.Cucciarelli,[32] J.A.van Dalen,[30] R.de Asmundis,[28] P.Déglon,[20] J.Debreczeni,[13] A.Degré,[4] K.Deiters,[45] D.della Volpe,[28] E.Delmeire,[20] P.Denes,[36] F.DeNotaristefani,[38] A.De Salvo,[47] M.Diemoz,[38] M.Dierckxsens,[2] D.van Dierendonck,[2] C.Dionisi,[38] M.Dittmar,[47,18] A.Doria,[28] M.T.Dova,[11,♯] D.Duchesneau,[4] P.Duinker,[2] B.Echenard,[20] A.Eline,[18] H.El Mamouni,[23] A.Engler,[34] F.J.Eppling,[14] A.Ewers,[1] P.Extermann,[20] M.A.Falagan,[24] S.Falciano,[38] A.Favara,[31] J.Fay,[23] O.Fedin,[33] M.Felcini,[47] T.Ferguson,[34] H.Fesefeldt,[1] E.Fiandrini,[32] J.H.Field,[20] F.Filthaut,[30] P.H.Fisher,[14] W.Fisher,[36] I.Fisk,[40] G.Forconi,[14] K.Freudenreich,[47] C.Furetta,[26] Yu.Galaktionov,[27,14] S.N.Ganguli,[10] P.Garcia-Abia,[5,18] M.Gataullin,[31] S.Gentile,[38] S.Giagu,[38] Z.F.Gong,[21] G.Grenier,[23] O.Grimm,[47] M.W.Gruenewald,[8,1] M.Guida,[39] R.van Gulik,[2] V.K.Gupta,[36] A.Gurtu,[10] L.J.Gutay,[44] D.Haas,[5] D.Hatzifotiadou,[9] T.Hebbeker,[8,1] A.Hervé,[18] J.Hirschfelder,[34] H.Hofer,[47] G. Holzner,[47] S.R.Hou,[49] Y.Hu,[30] B.N.Jin,[7] L.W.Jones,[3] P.de Jong,[2] I.Josa-Mutuberría,[24] D.Käfer,[1] M.Kaur,[15] M.N.Kienzle-Focacci,[20] J.K.Kim,[42] J.Kirkby,[18] W.Kittel,[30] A.Klimentov,[14,27] A.C.König,[30] M.Kopal,[44] V.Koutsenko,[14,27] M.Kräber,[47] R.W.Kraemer,[34] W.Krenz,[1] A.Krüger,[46] A.Kunin,[14] P.Ladron de Guevara,[24] I.Laktineh,[23] G.Landi,[17] M.Lebeau,[18] A.Lebedev,[14] P.Lebrun,[23] P.Lecomte,[47] P.Lecoq,[18] P.Le Coultre,[47] H.J.Lee,[8] J.M.Le Goff,[18] R.Leiste,[46] P.Levtchenko,[33] C.Li,[21] S.Likhoded,[46] C.H.Lin,[49] W.T.Lin,[49] F.L.Linde,[2] L.Lista,[28] Z.A.Liu,[7] W.Lohmann,[46] E.Longo,[38] Y.S.Lu,[7] K.Lübelsmeyer,[1] C.Luci,[38] L.Luminari,[38] W.Lustermann,[47] W.G.Ma,[21] L.Malgeri,[20] A.Malinin,[27] C.Maña,[24] D.Mangeol,[30] J.Mans,[36] J.P.Martin,[23] F.Marzano,[38] K.Mazumdar,[10] R.R.McNeil,[6] S.Mele,[18,28] L.Merola,[28] M.Meschini,[17] W.J.Metzger,[30] A.Mihul,[12] H.Milcent,[18] G.Mirabelli,[38] J.Mnich,[1] G.B.Mohanty,[10] G.S.Muanza,[23] A.J.M.Muijs,[2] B.Musicar,[40] M.Musy,[38] S.Nagy,[16] M.Napolitano,[28] F.Nessi-Tedaldi,[47] H.Newman,[31] T.Niessen,[1] A.Nisati,[38] H.Nowak,[46] R.Ofierzynski,[47] G.Organtini,[38] C.Palomares,[18] D.Pandoulas,[1] P.Paolucci,[28] R.Paramatti,[38] G.Passaleva,[17] S.Patricelli,[28] T.Paul,[11] M.Pauluzzi,[32] C.Paus,[14] F.Pauss,[47] M.Pedace,[38] S.Pensotti,[26] D.Perret-Gallix,[4] B.Petersen,[30] D.Piccolo,[28] F.Pierella,[9] M.Pioppi,[32] P.A.Piroué,[36] E.Pistolesi,[26] V.Plyaskin,[27] M.Pohl,[20] V.Pojidaev,[17] J.Pothier,[18] D.O.Prokofiev,[44] D.Prokofiev,[33] J.Quartieri,[39] G.Rahal-Callot,[47] M.A.Rahaman,[10] P.Raics,[16] N.Raja,[10] R.Ramelli,[47] P.G.Rancoita,[26] R.Ranieri,[17] A.Raspereza,[46] P.Razis,[29]D.Ren,[47] M.Rescigno,[38] S.Reucroft,[11] S.Riemann,[46] K.Riles,[3] B.P.Roe,[3] L.Romero,[24] A.Rosca,[8] S.Rosier-Lees,[4] S.Roth,[1] C.Rosenbleck,[1] B.Roux,[30] J.A.Rubio,[18] G.Ruggiero,[17] H.Rykaczewski,[47] A.Sakharov,[47] S.Saremi,[6] S.Sarkar,[38] J.Salicio,[18] E.Sanchez,[24] M.P.Sanders,[30] C.Schäfer,[18] V.Schegelsky,[33] S.Schmidt-Kaerst,[1] D.Schmitz,[1] H.Schopper,[48] D.J.Schotanus,[30] G.Schwering,[1] C.Sciacca,[28] L.Servoli,[32] S.Shevchenko,[31] N.Shivarov,[41] V.Shoutko,[14] E.Shumilov,[27] A.Shvorob,[31] T.Siedenburg,[1] D.Son,[42] P.Spillantini,[17] M.Steuer,[14] D.P.Stickland,[36] B.Stoyanov,[41] A.Straessner,[18] K.Sudhakar,[10] G.Sultanov,[41] L.Z.Sun,[21] S.Sushkov,[8] H.Suter,[47] J.D.Swain,[11] Z.Szillasi,[25,¶] X.W.Tang,[7] P.Tarjan,[16] L.Tauscher,[5] L.Taylor,[11] B.Tellili,[23] D.Teyssier,[23] C.Timmermans,[30] Samuel C.C.Ting,[14] S.M.Ting,[14] S.C.Tonwar,[10,18] J.Tóth,[13] C.Tully,[36] K.L.Tung,[7] J.Ulbricht,[47] E.Valente,[38] R.T.Van de Walle,[30] V.Veszpremi,[25] G.Vesztergombi,[13] I.Vetlitsky,[27] D.Vicinanza,[39] G.Viertel,[47] S.Villa,[37] M.Vivargent,[4] S.Vlachos,[5] I.Vodopianov,[33] H.Vogel,[34] H.Vogt,[46] I.Vorobiev,[3427] A.A.Vorobyov,[33] M.Wadhwa,[5] W.Wallraff,[1] X.L.Wang,[21] Z.M.Wang,[21] M.Weber,[1] P.Wienemann,[1] H.Wilkens,[30] S.Wynhoff,[36] L.Xia,[31] Z.Z.Xu,[21] J.Yamamoto,[3] B.Z.Yang,[21] C.G.Yang,[7] H.J.Yang,[3] M.Yang,[7] S.C.Yeh,[50] An.Zalite,[33] Yu.Zalite,[33] Z.P.Zhang,[21] J.Zhao,[21] G.Y.Zhu,[7] R.Y.Zhu,[31] H.L.Zhuang,[7] A.Zichichi,[9,18,19] G.Zilizi,[25,¶] B.Zimmermann,[47] M.Zöller.[1]

1 I. Physikalisches Institut, RWTH, D-52056 Aachen, FRG[§]
III. Physikalisches Institut, RWTH, D-52056 Aachen, FRG[§]
2 National Institute for High Energy Physics, NIKHEF, and University of Amsterdam, NL-1009 DB Amsterdam, The Netherlands
3 University of Michigan, Ann Arbor, MI 48109, USA
4 Laboratoire d'Annecy-le-Vieux de Physique des Particules, LAPP,IN2P3-CNRS, BP 110, F-74941 Annecy-le-Vieux CEDEX, France
5 Institute of Physics, University of Basel, CH-4056 Basel, Switzerland
6 Louisiana State University, Baton Rouge, LA 70803, USA
7 Institute of High Energy Physics, IHEP, 100039 Beijing, China[△]
8 Humboldt University, D-10099 Berlin, FRG[§]
9 University of Bologna and INFN-Sezione di Bologna, I-40126 Bologna, Italy
10 Tata Institute of Fundamental Research, Mumbai (Bombay) 400 005, India
11 Northeastern University, Boston, MA 02115, USA
12 Institute of Atomic Physics and University of Bucharest, R-76900 Bucharest, Romania
13 Central Research Institute for Physics of the Hungarian Academy of Sciences, H-1525 Budapest 114, Hungary[‡]
14 Massachusetts Institute of Technology, Cambridge, MA 02139, USA
15 Panjab University, Chandigarh 160 014, India.
16 KLTE-ATOMKI, H-4010 Debrecen, Hungary[¶]
17 INFN Sezione di Firenze and University of Florence, I-50125 Florence, Italy
18 European Laboratory for Particle Physics, CERN, CH-1211 Geneva 23, Switzerland
19 World Laboratory, FBLJA Project, CH-1211 Geneva 23, Switzerland
20 University of Geneva, CH-1211 Geneva 4, Switzerland
21 Chinese University of Science and Technology, USTC, Hefei, Anhui 230 029, China[△]
22 University of Lausanne, CH-1015 Lausanne, Switzerland
23 Institut de Physique Nucléaire de Lyon, IN2P3-CNRS,Université Claude Bernard, F-69622 Villeurbanne, France
24 Centro de Investigaciones Energéticas, Medioambientales y Tecnologícas, CIEMAT, E-28040 Madrid, Spain[♭]
25 Florida Institute of Technology, Melbourne, FL 32901, USA
26 INFN-Sezione di Milano, I-20133 Milan, Italy
27 Institute of Theoretical and Experimental Physics, ITEP, Moscow, Russia
28 INFN-Sezione di Napoli and University of Naples, I-80125 Naples, Italy
29 Department of Physics, University of Cyprus, Nicosia, Cyprus
30 University of Nijmegen and NIKHEF, NL-6525 ED Nijmegen, The Netherlands
31 California Institute of Technology, Pasadena, CA 91125, USA
32 INFN-Sezione di Perugia and Università Degli Studi di Perugia, I-06100 Perugia, Italy
33 Nuclear Physics Institute, St. Petersburg, Russia
34 Carnegie Mellon University, Pittsburgh, PA 15213, USA
35 INFN-Sezione di Napoli and University of Potenza, I-85100 Potenza, Italy
36 Princeton University, Princeton, NJ 08544, USA
37 University of Californa, Riverside, CA 92521, USA
38 INFN-Sezione di Roma and University of Rome, "La Sapienza", I-00185 Rome, Italy
39 University and INFN, Salerno, I-84100 Salerno, Italy
40 University of California, San Diego, CA 92093, USA
41 Bulgarian Academy of Sciences, Central Lab. of Mechatronics and Instrumentation, BU-1113 Sofia, Bulgaria
42 The Center for High Energy Physics, Kyungpook National University, 702-701 Taegu, Republic of Korea
43 Utrecht University and NIKHEF, NL-3584 CB Utrecht, The Netherlands
44 Purdue University, West Lafayette, IN 47907, USA
45 Paul Scherrer Institut, PSI, CH-5232 Villigen, Switzerland
46 DESY, D-15738 Zeuthen, FRG
47 Eidgenössische Technische Hochschule, ETH Zürich, CH-8093 Zürich, Switzerland
48 University of Hamburg, D-22761 Hamburg, FRG
49 National Central University, Chung-Li, Taiwan, China
50 Department of Physics, National Tsing Hua University, Taiwan, China
§ Supported by the German Bundesministerium für Bildung, Wissenschaft, Forschung und Technologie
‡ Supported by the Hungarian OTKA fund under contract numbers T019181, F023259 and T024011.
¶ Also supported by the Hungarian OTKA fund under contract number T026178.
♭ Supported also by the Comisión Interministerial de Ciencia y Tecnología.
♯ Also supported by CONICET and Universidad Nacional de La Plata, CC 67, 1900 La Plata, Argentina.
△ Supported by the National Natural Science Foundation of China.

p_t [GeV]	$\langle p_t \rangle$ [GeV]	Efficiency [%]	$d\sigma/dp_t$ for $W_{\gamma\gamma} > 5$ GeV [pb/GeV]	$d\sigma/dp_t$ for $W_{\gamma\gamma} > 10$ GeV [pb/GeV]
0.2−0.4	0.28	12.9 ± 1.2	(89 ± 1 ± 8) $\times 10^2$	(62 ± 0.8 ± 6) $\times 10^2$
0.4−0.6	0.48	24.3 ± 2.2	(44 ± 0.3 ± 4) $\times 10^2$	(35 ± 0.3 ± 3) $\times 10^2$
0.6−0.8	0.68	30.7 ± 2.8	(18 ± 0.1 ± 2) $\times 10^2$	(15 ± 0.1 ± 1) $\times 10^2$
0.8−1.0	0.88	35.4 ± 3.2	(73 ± 0.8 ± 7) $\times 10^1$	(59 ± 0.7 ± 6) $\times 10^1$
1.0−1.5	1.14	37.2 ± 3.4	(22 ± 0.3 ± 2) $\times 10^1$	(18 ± 0.3 ± 2) $\times 10^1$
1.5−2.0	1.68	37.4 ± 3.5	(46 ± 1 ± 4)	(40 ± 1 ± 4)
2.0−3.0	2.31	35.8 ± 3.5	(11 ± 0.5 ± 1)	(95 ± 5 ± 11) $\times 10^{-1}$
3.0−4.0	3.36	23.5 ± 4.1	(30 ± 6 ± 5) $\times 10^{-1}$	
4.0−5.0	4.39	47.5 ± 8.5	(76 ± 14 ± 1) $\times 10^{-2}$	
5.0−7.5	5.79	26.7 ± 3.0	(26 ± 4 ± 3) $\times 10^{-2}$	
7.5−10.0	8.46	26.4 ± 3.7	(73 ± 18 ± 10) $\times 10^{-3}$	
10.0−15.0	11.98	21.7 ± 3.9	(27 ± 9 ± 5) $\times 10^{-3}$	
15.0−20.0	17.36	15.6 ± 3.8	(14 ± 8 ± 4) $\times 10^{-3}$	

Table 1: The π^0 overall efficiency and differential cross sections as a function of p_t for $|\eta| < 0.5$. For $p_t < 4$ GeV, the π^0 is only reconstructed from its decay into two photons. Above 5 GeV, the π^0 is only detected as a single cluster. In the $4 - 5$ GeV bin, both methods are used yielding a higher efficiency. The first uncertainty on cross sections is statistical and the second one systematic. The cross sections are calculated for $W_{\gamma\gamma} > 5$ GeV and $W_{\gamma\gamma} > 10$ GeV and coincide for $p_t > 3$ GeV.

Detector	$\lvert\eta\rvert$	Number of π^0	Efficiency [%]	$d\sigma/d\lvert\eta\rvert$ [pb]
Barrel	0.0−0.2	8914	35.6 ± 4.0	303 ± 8 ± 33
	0.2−0.4	9263	36.7 ± 4.1	305 ± 8 ± 33
	0.4−0.6	8965	34.2 ± 3.8	317 ± 8 ± 34
	0.6−0.8	8094	31.7 ± 3.6	308 ± 8 ± 33
Endcap	0.8−1.4	8688	12.4 ± 2.1	282 ± 10 ± 47
	1.4−1.6	3443	16.6 ± 2.9	251 ± 15 ± 42
	1.6−1.8	3050	16.4 ± 3.0	225 ± 15 ± 37
	1.8−2.0	2313	15.2 ± 2.8	184 ± 15 ± 31
	2.0−2.2	2294	12.7 ± 2.5	217 ± 23 ± 36
Small-angle	3.4−4.3	1410	16.4 ± 3.5	23 ± 2 ± 5

Table 2: The number of reconstructed π^0, overall efficiency and differential cross section as a function of pseudorapidity for $p_t > 1$ GeV and $W_{\gamma\gamma} > 5$ GeV. The first uncertainty on the cross section is statistical and the second one systematic.

p_t [GeV]	$\langle p_t \rangle$ [GeV]	Efficiency [%]	$d\sigma/dp_t$ for $W_{\gamma\gamma} > 5$ GeV [pb/GeV]	$d\sigma/dp_t$ for $W_{\gamma\gamma} > 10$ GeV [pb/GeV]
0.4−0.6	0.49	13.6 ± 0.1	1522 ± 20 ± 81	1262 ± 21 ± 65
0.6−0.8	0.69	17.8 ± 0.2	947 ± 14 ± 53	786 ± 16 ± 40
0.8−1.0	0.89	20.0 ± 0.3	521 ± 11 ± 27	428 ± 12 ± 22
1.0−1.5	1.16	22.2 ± 0.4	180 ± 5 ± 9	151 ± 4 ± 8
1.5−2.0	1.67	22.4 ± 1.0	46 ± 3 ± 3	42 ± 2 ± 2
2.0−3.0	2.29	16.1 ± 1.3	10 ± 1 ± 0.6	11 ± 1 ± 0.6
3.0−4.0	3.35	14.8 ± 4.8	2.1 ± 0.8 ± 0.2	1 ± 0.5 ± 0.3

Table 3: The K^0_S overall efficiency and differential cross sections as a function of p_t for $|\eta| < 1.5$. The first uncertainty on cross section is statistical and the second one systematic. The cross section is calculated for $W_{\gamma\gamma} > 5$ GeV and $W_{\gamma\gamma} > 10$ GeV.

$\lvert\eta\rvert$	Number of K^0_S	Efficiency [%]	$d\sigma/d\lvert\eta\rvert$[pb]
0.0−0.3	744	23.3 ± 0.8	25.9 ± 2.0 ± 1.3
0.3−0.6	759	24.5 ± 0.8	25.1 ± 1.9 ± 1.2
0.6−1.5	1473	14.7 ± 1.2	27.1 ± 2.4 ± 3.2

Table 4: The number of reconstructed K^0_S, overall efficiency and differential cross section as a function of pseudorapidity for $p_t > 1.5$ GeV and $W_{\gamma\gamma} > 5$ GeV. The first uncertainty on the cross section is statistical and the second one systematic.

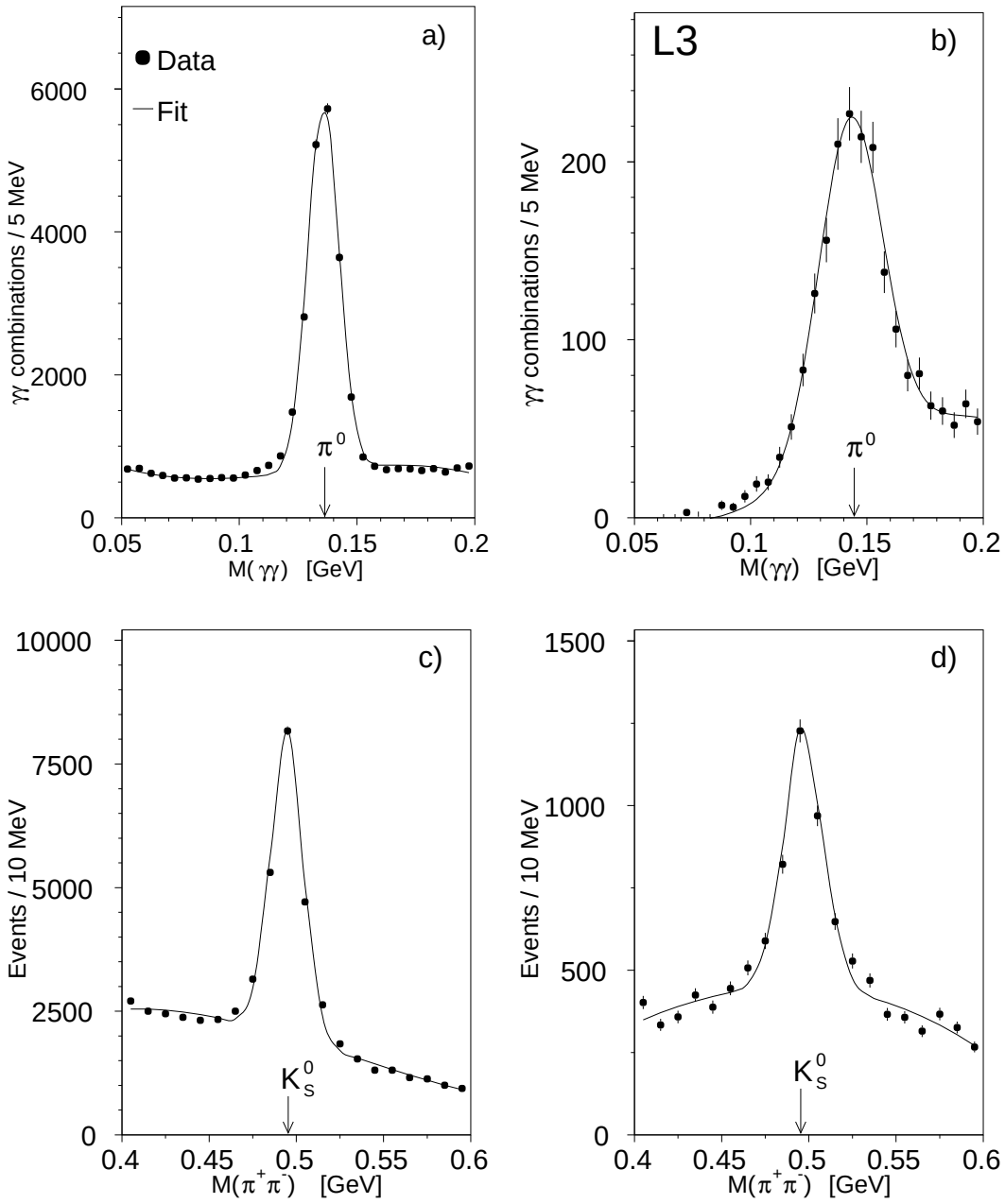

Figure 1: Two photon effective mass for a) $1 < p_t < 1.5$ GeV in the central region and b) for $p_t > 0.2$ GeV in the small angle detector. Two charged pion effective mass for c) $0.2 < p_t < 0.4$ GeV and d) $0.8 < p_t < 1.0$ GeV. The π^0 and K^0_S peaks are fitted with a Gaussian and the background with a Chebyshev polynomial. Values of the π^0 and K^0_S masses are also indicated.

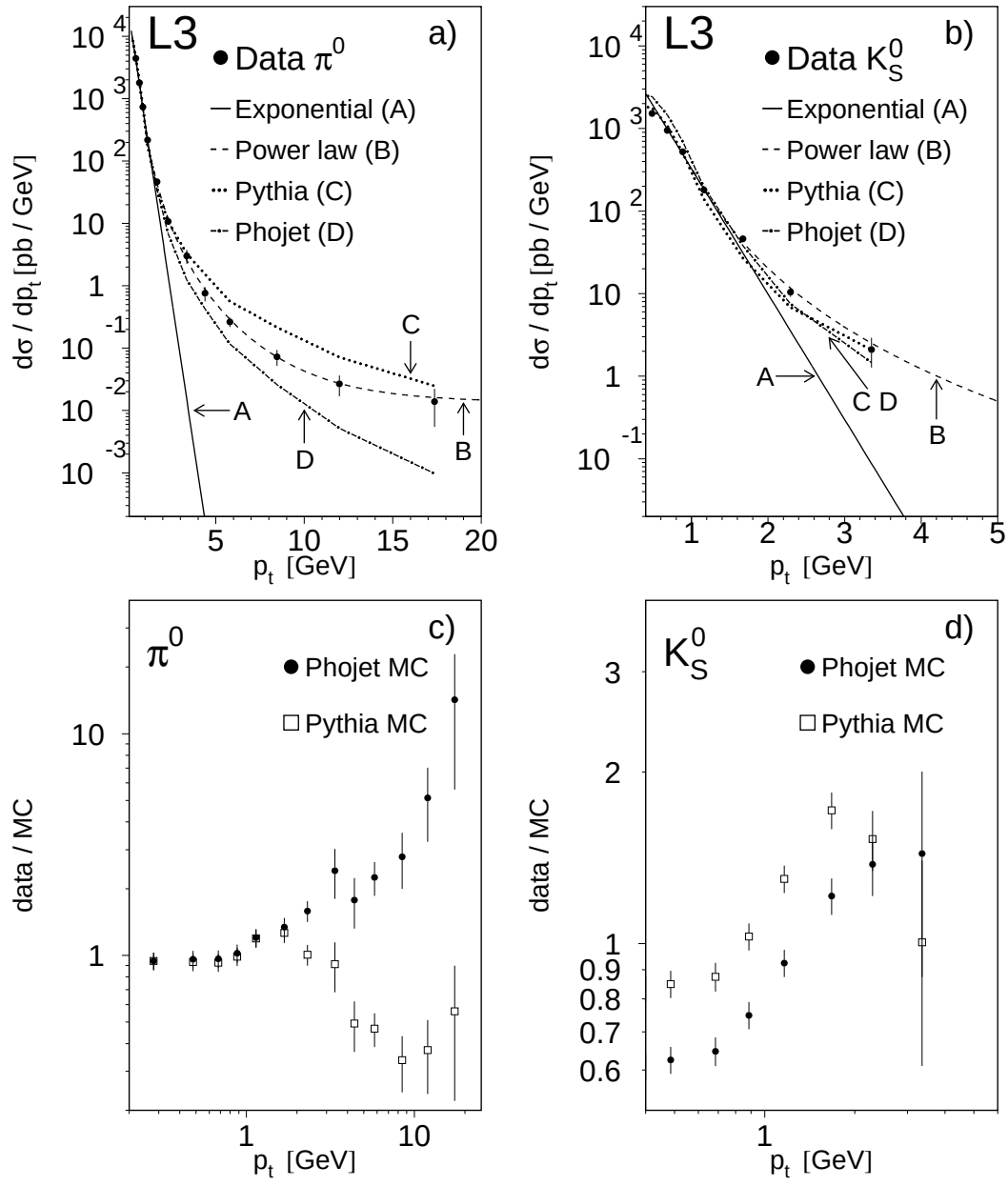

Figure 2: Inclusive differential cross section $d\sigma/dp_t$ compared to Monte Carlo predictions and exponential and power law behaviour for: a) π^0 production for $|\eta|$ <0.5 and b) K^0_S production for $|\eta| < 1.5$. Ratio of the differential cross section $d\sigma/dp_t$ to Monte Carlo predictions for: c) π^0 production and d) K^0_S production.

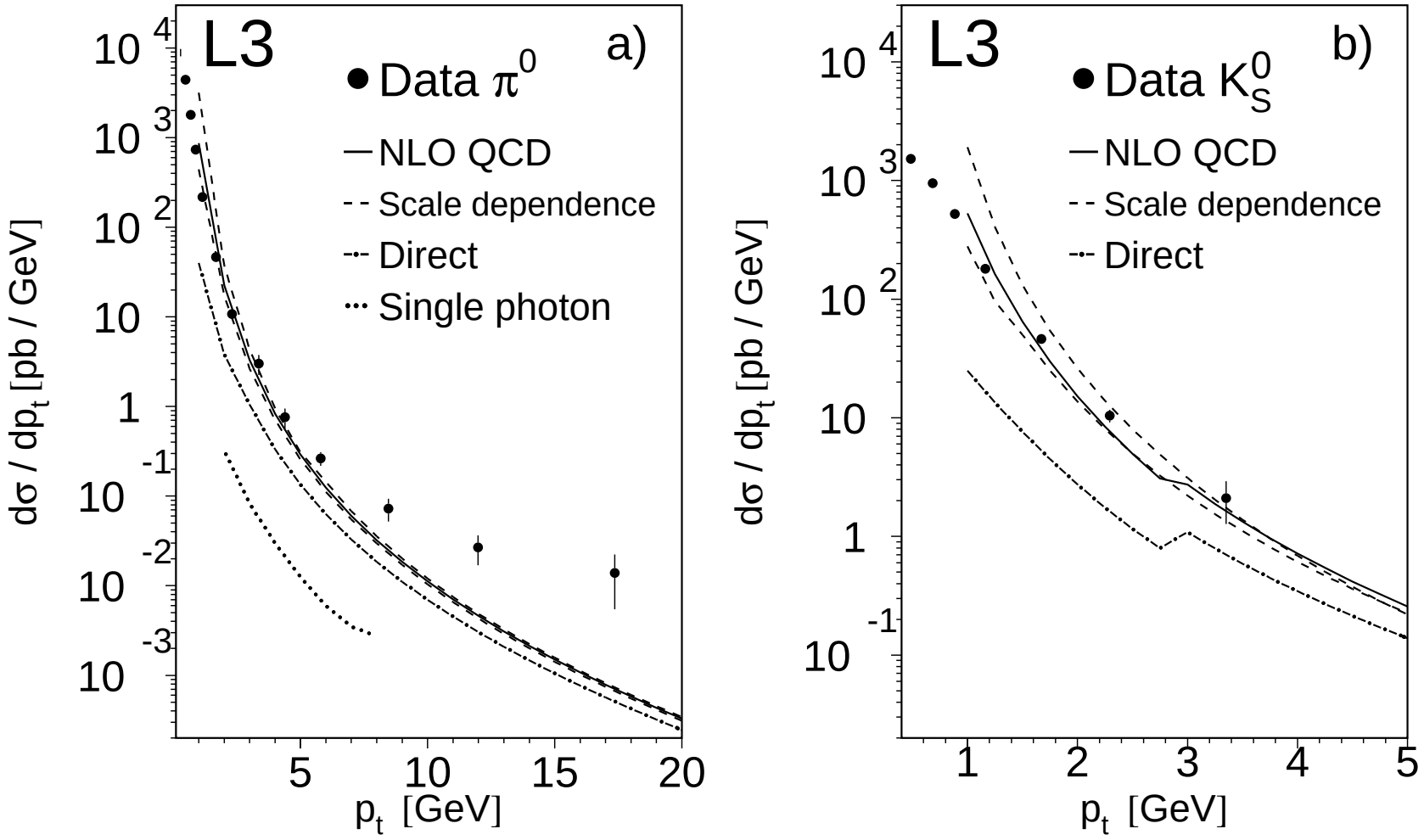

Figure 3: Inclusive differential cross section $d\sigma/dp_t$ compared to NLO QCD predictions for: a) π^0 production for $|\eta| < 0.5$ and b) K^0_S production for $|\eta| < 1.5$. The NLO calculations are given for the QCD scale equal to p_t (full line) and for the scales 0.5 p_t (upper dashed line) and 2 p_t (lower dashed line). The contribution of the direct QED process is indicated as a dashed dotted line. For the π^0 case the estimation of the single photon production [16] is indicated as a dotted line. The structure at 3GeV in b) is due to the charm threshold in the fragmentation function [2,22].

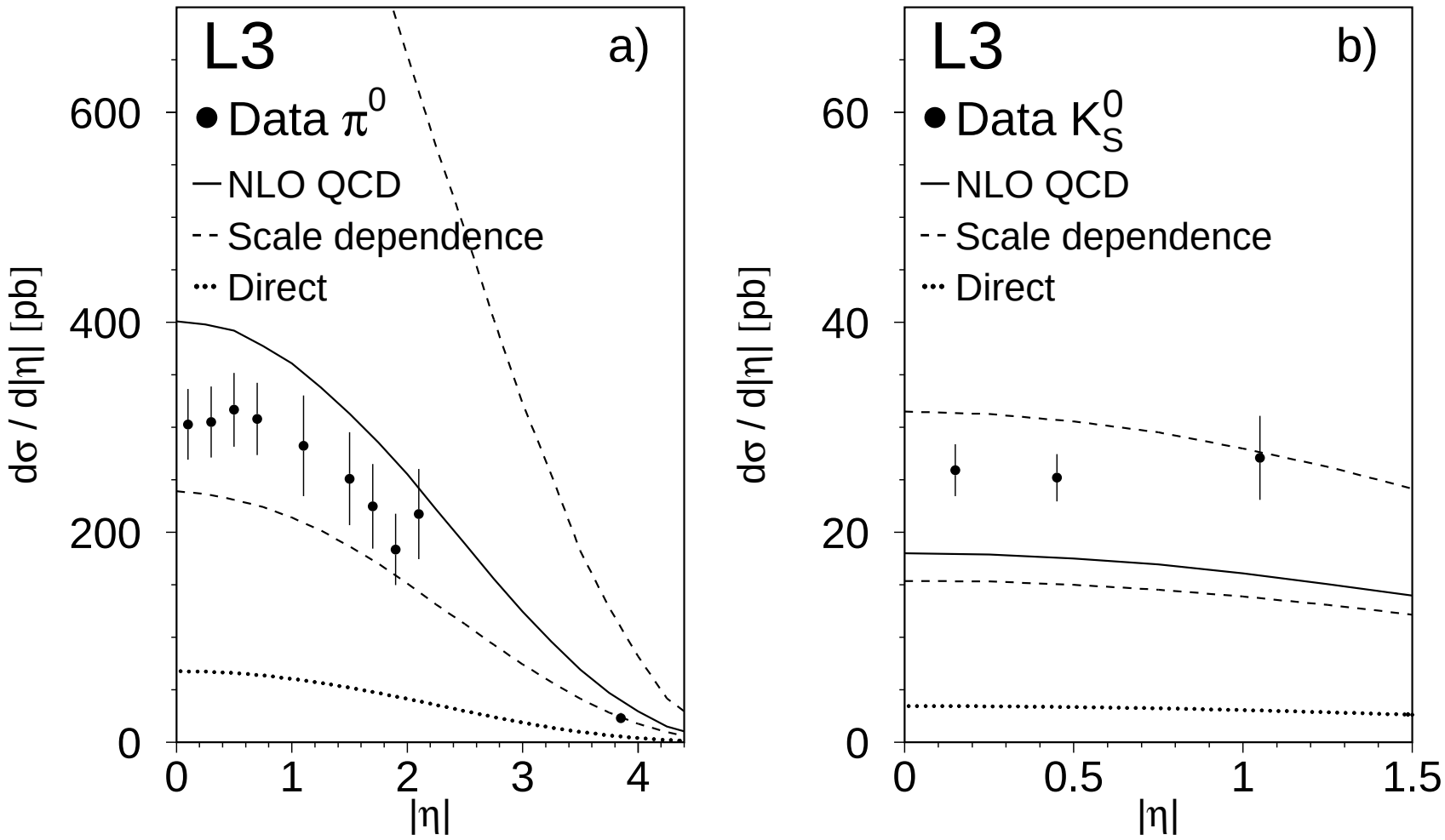

Figure 4: Inclusive differential cross sections $d\sigma/d|\eta|$ compared to NLO QCD predictions for: a) π^0 production for $p_t > 1$ GeV and b) K^0_S production for $p_t > 1.5$ GeV. The NLO calculations are given for the QCD scale equal to p_t (full line) and for the scales 0.5 p_t (upper dashed line) and 2 p_t (lower dashed line). The contribution of the direct QED process is indicated as a dotted line.